

Absolute cross sections and final-state distributions for dissociative recombination and excitation of $\text{CO}^+(v=0)$ using an ion storage ring

S. Rosén,¹ R. Peverall,² M. Larsson,¹ A. Le Padellec,³ J. Semaniak,^{3,4} Å. Larson,³ C. Strömholm,⁵ W. J. van der Zande,² H. Danared,⁵ and G. H. Dunn^{5,6}

¹*Department of Physics, Stockholm University, P.O. Box 6730, S-11385 Stockholm, Sweden*

²*FOM Institute for Atomic and Molecular Physics, Kruislaan 407, 1098 SJ Amsterdam, The Netherlands*

³*Department of Physics I, Royal Institute of Technology, S-10044 Stockholm, Sweden*

⁴*Institute of Physics, Pedagogical University, ulica Lesna 16, 25-509 Kielce, Poland*

⁵*Manne Siegbahn Laboratory, Stockholm University, S-10405 Stockholm, Sweden*

⁶*JILA, University of Colorado, Boulder, Colorado 80309-0440*

(Received 20 October 1997)

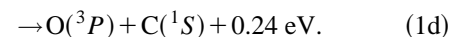
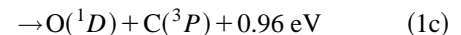
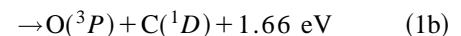
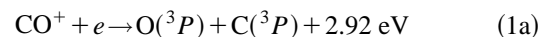
Absolute cross sections and rate coefficients have been determined for dissociative recombination of electrons and CO^+ ions for energies from 1 meV to 54 eV. We found values of $4 \times 10^{-12} \text{ cm}^2$ at 1 meV and 10^{-15} cm^2 at 1 eV, with an essentially $1/E$ energy dependence. Branching ratios over the final atomic product states have been determined using a position- and time-sensitive imaging system. At zero eV collision energy the predominant yield is to ground-state atomic fragments (76%). At higher collisional energies the branching ratio to the ground-state limit is reduced. A new limit, $\text{O}(^1D) + \text{C}(^1D)$, opens up and branching to the $\text{O}(^3P) + \text{C}(^1D)$ limit increases. Cross sections are also determined for dissociative excitation of CO^+ . Thermal rate coefficients are deduced from the dissociative recombination (DR) data, and compared with measurements in the literature. Consideration of both the theoretical and spectroscopic data in the literature giving information about the potential curves along which DR may take place reveals both a paucity and disparity of the data. [S1050-2947(98)06806-1]

PACS number(s): 34.80.Gs, 34.80.Kw, 34.80.Lx

I. INTRODUCTION

Carbon monoxide (CO) is the second most abundant molecule in the universe after molecular hydrogen, and it is present in a wide variety of astrophysical environments, from the hot diffuse clouds to the denser and colder molecular clouds such as the dark clouds and the giant molecular complexes associated with H II regions. Since H_2 is not directly observable, CO is used as a tracer to map the molecular hydrogen in the Milky Way as well as in other galaxies, a procedure performed basically by means of millimeter radio astronomy techniques. Observations also show CO in other astrophysical objects such as circumstellar envelopes, bipolar flows associated with birthplaces of stars, and planetary or cometary atmospheres. In all these media, its abundance with respect to H_2 is determined mainly by the photodissociation rate in the ambient UV radiation field. On the other hand, singly charged carbon monoxide has been detected so far in only a few astrophysical environments, for instance toward the interfaces between molecular clouds and H II regions around massive O stars [1,2]. In addition, its abundance compared with other ions was determined to be rather small, which can be understood in the framework of fast conversion of CO^+ into HCO^+ by reaction with H_2 . Hence, CO^+ is usually of significant abundance only in the hot layers of photon-dominated regions (called PDR's), where a significant fraction of hydrogen is present in atomic form. Very recently, CO^+ was also detected toward a PDR associated with the reflection nebula NGC7023, in the vicinity of a Be star [3]. Its presence in such an environment remains mysterious, since a Be star cannot provide the photons to photoionize CO.

From the above, it follows that detailed knowledge of the different pathways leading to the formation as well as to the destruction of CO^+ is needed. This publication presents data on the destruction through dissociative recombination (DR). Our findings suggest that DR is an efficient process. Already two decades ago, this process was invoked in a model of carbon production in cometary ionospheres [4]. At that time, ultraviolet spectra revealed a substantial amount of resonance scattering at 193.1 nm from metastable $\text{C}(^1D)$ atoms [5] (lifetime 3200 s) from the ionospheres of the comets Kahoutek (1973) and West (1976). Since the dominant destruction mechanism for CO was thought to be photoionization rather than photodissociation, Feldman suggested that the DR of the CO^+ ions could be a source of the metastable carbon atoms according to the second of the four exothermic channels [4]:



The energies of these reactions pertain to CO^+ in its ground vibrational state and at zero eV collision energy. Feldman [4] used in his model calculations a value for the DR thermal rate coefficient of $3 \times 10^{-7} \text{ cm}^3 \text{ s}^{-1}$ at 300 K (this happens to be close to the value measured in this paper). He also assumed the branching ratio (1b) to be unity in order to fit the $\text{C}(^1D)$ from the comet West (this we found to be incorrect).

In comets, dissociative recombination may not be the only destruction pathway. The ion CO^+ reacts also with H_2O , and water is another abundant cometary compound. The presence of CO^+ was established in the outer coma of comet Halley [6]. In the latter observation, neither the dissociative photoionization of CO , CO_2 , nor CH_4 , nor the photodissociation of these molecules followed by photoionization of carbon atoms could account for the measured abundance of C^+ . No mention was made of DR as a mechanism to provide the carbon atoms that in turn would be photoionized. Given the large DR rates reported in the present paper, the role of DR in C^+ formation may be readdressed.

A different issue is the escape of carbon and oxygen and their compounds from Mars in time, McElroy, Kong, and Young [7] mentioned the DR of CO^+ , as a mechanism to produce sufficiently fast carbon and oxygen atoms. Escape due to dissociative recombination seems well established for the case of N_2^+ [8]. This mechanism may even explain the difference between Earth and Mars of the isotopic ratio ^{15}N to ^{14}N , because of a preferential escape of the lighter ^{14}N isotope from the martian atmosphere [9].

This paper also presents the result of dissociative excitation (DE), which has an onset at an electron energy of 12.5 eV.

The experiments presented in this paper were carried out at the heavy-ion storage ring CRYRING, located at the Manne Siegbahn Laboratory at Stockholm University. The remainder of the paper is organized as follows. The experimental description and the analysis procedure are given in Sec. II. Section III describes the observed dissociative recombination cross sections, the final state product branching ratios, and dissociative excitation cross sections. Section IV provides further discussion of the DR results, comparing them with earlier thermal rate measurements and discussing pathways and mechanisms for the processes.

II. EXPERIMENT

The experiments have been performed at the CRYRING (CRYogenic RING) heavy-ion storage ring at the Manne Siegbahn Laboratory. A stored circulating ion beam is merged with an electron beam over a known distance and with a variable relative energy. The rate of neutral production by electron-molecular ion interactions is used to extract the rate coefficient of the process under study. An imaging detector is applied to extract final state information of the atomic fragments. The storage ring and data analysis procedure were described in detail in previous publications [10–12], so that only the main features will be given here.

A. Cryring

A CO^+ ion beam was produced in a hot-cathode discharge ion source (MINIS) with an energy of 40 keV. To avoid possible contamination with N_2^+ ions (same mass to charge ratio, A/q), we chose to study $^{13}\text{C}^{16}\text{O}^+$ produced from electron impact of $^{13}\text{C}^{16}\text{O}$. After mass selection, the ions were injected into the ring and further accelerated to an energy of 0.116 MeV per atomic mass unit, which corresponds to a full CO^+ energy (FE) of 3.423 MeV. At each passage through the electron cooler region, the ions inter-

acted over a distance of 85 cm with a 64.7-eV, 1.45-mA, 4-cm-diam continuously renewed electron beam. Electron cooling [13], that is the reduction of the phase space of the ion beam by momentum transfer between the ‘‘cold’’ electron beam and the ‘‘hotter’’ ion beam, was not efficient within the time scale of the experiment. The ion beam half-life time of about 1.75 s was, however, large enough to allow the data acquisition.

During the data acquisition, the velocity of the electron beam is changed so that electron-ion collisions at well-defined center-of-mass collision energies are obtained. The difference between the velocities of the ion and electron beams is called the detuning energy ν_d , and is associated, nonrelativistically, with the detuning energy according to $E_d = m_e \nu_d^2 / 2$. In the initial, ‘‘cooling’’ phase of an injection cycle the detuning velocity is zero. After about 5 s, the electron beam velocity is changed so that ν_d becomes different from zero. These electron cooler jumps are performed five times per injection cycle during time windows of 200 ms, and always to the same detuning energy. After 10–15 min the measurement is terminated; the electron cooler is now set to jump to a different detuning energy, and a new set of data is recorded. The spread in the noncooled ion velocities of approximately ($\Delta v/v = 10^{-3}$) does not contribute significantly to the spread in collision energies. The contribution to the energy spread is 25 meV at 10 eV, 2.5 meV at 0.1 eV, and 0.25 meV at 1 meV relative collision energy. Thus, the spread in collision energies is entirely dominated by the transverse ($kT_{\perp} = 10$ meV) and longitudinal ($kT_{\parallel} = 0.1$ meV) energy spreads in the electron beam [10]. The center-of-mass collision energy is not well defined for energies below kT_{\perp} . When E_d is larger than kT_{\perp} , the center-of-mass energy approaches the detuning energy. It is noteworthy that the detuning energy can be smaller than kT_{\perp} . We have followed common practice and used the detuning energy as the energy scale.

The storage time ensured that the CO^+ ions are in their electronic and vibrational ground states. The $\text{CO}^+(X^2\Sigma^+)$ ions have a sizable dipole moment of 2.77 D; vibrationally excited molecules can fully relax to the ground state by infrared radiation. Electronically excited states also have relaxed in our experiment. Such contaminations (see the later discussion of dissociative excitation DE) may have occurred in previous single-pass experiments by Mitchell and Hus [14]. According to Desqueselles, Dufay, and Poulizac [15] and to Bennett and Dalby [16], the $B^2\Sigma^+$ state has a mean lifetime of 45 ns and is thus of no concern. The $A^2\Pi$ state decays much more slowly than the B state, with lifetimes that were measured [17–19] for individual vibrational levels ranging from 3.82 μs ($v=0$) to 2.10 μs ($v=9$). In our case, measurements did not begin until 3 s after injection of the ions. The present results definitely relate to the $\text{CO}^+(X^2\Sigma^+, v=0)$ ground state, a fact that was confirmed by the three-dimensional imaging data (see Sec. III B).

DR and DE events were observed by detecting the neutral fragments produced within the interaction region (in the present case C and O). These product neutrals leave the storage ring at the first dipole magnet located downstream of the electron cooler and enter the so-called 0° arm. In this arm are located both an energy-sensitive surface barrier detector (SBD) and a three-dimensional imaging detector to study the kinetic energy released in the center-of-mass frame.

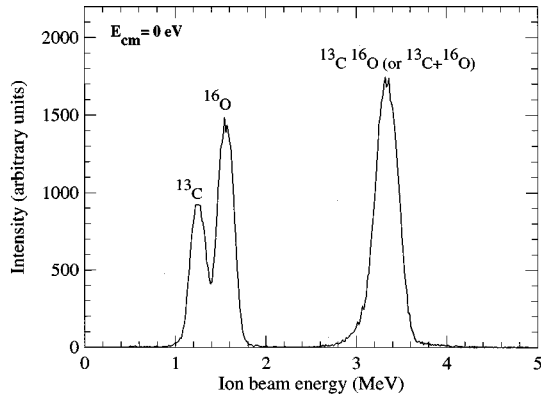


FIG. 1. MCA spectrum. The peak at full beam energy (FE) of 3.4 MeV, P_3 , reflects the DR signal. The peaks at lower energy are due to collisional background P_{12} .

B. Data analysis procedure

Figure 1 displays a typical multichannel analyzer (MCA) spectrum (recorded during a number of time gates in each injection cycle) with three different peaks corresponding, respectively, to the C fragments (energy equals $\frac{13}{29}$ FE), the O fragments (16/29 FE) and the C+O (or CO) fragments (energy equals FE). The data protocol described previously [10] was used here, wherein the ion current is measured only once during the measurement while simultaneous measurements were made of the FE peak and the fractional FE or “background” peaks. The background peaks were then used throughout the rest of the experiment as indicators of the magnitude of the ion current in the ring. In this experiment, the C and O fragment peaks were unfortunately not completely resolved, i.e., the SBD peaks overlapped each other, see Fig. 1. Thus, for the background peak, we combined the C and O fragment peaks. The label P_{12} pertains to the integrated number of counts in that combination peak, and we denote the integrated number of counts in the full energy peak (DR) by P_3 . The integrated number of counts P_{12} and P_3 obtained from the MCA spectra contain unwanted contributions, leading to the subscript “cor” in Eq. (2). $P_{12\text{cor}}$ and $P_{3\text{cor}}$ are thus the integrated number of counts after correction, described as follows. Charge transfer between the rest gas (mainly H_2) and CO^+ gives nonsignal counts in P_3 . This is quantified by recording this peak in a multichannel scaler (MCS) spectrum (recorded during the whole injection cycle) whilst turning the electrons on and off [12]. The background peak P_{12} is affected at elevated collision energies by DE and quantified recording the background count rate using the MCS. A small background comes from positive ions trapped in the electron beam. The amount of trapped ions changes with electron energy since the ionization cross section varies with electron energy. The contribution to the count rate in the background peaks from trapped ions was observed while switching the electrons on an off ($E_d=0$ eV) while monitoring the P_{12} peak in an MCS measurement. The “trapping effect” was found to contribute very little to P_{12} in these measurements. It has been shown [10] that the absolute DR rate coefficient (in units of $\text{cm}^3 \text{s}^{-1}$) is given by the simple relation

$$R_{\text{DR}} = R_B \left[\frac{C}{n_e L} \right] \frac{P_{3\text{cor}}}{P_{12\text{cor}}}. \quad (2)$$

The circumference of the ring and the length of the interaction region are respectively $C=51.6$ and $L=0.85$ m, and the electron density is n_e . The electron beam is run in a fixed current and diameter mode, so that n_e decreases inversely as the velocity of the electrons. The rest gas destruction rate per ion and unit time is R_B and is proportional to the ratio of the background count rate dP_{12}/dt to the absolute ion current, both recorded at the same time. R_B was found to be $13.5 \times 10^{-3} \text{ s}^{-1}$.

The DE rates were obtained by subtracting the contribution due to rest-gas collisions from the observed background counts P_{12} . The increase in count rate was measured applying electron cooler jumps in an MCS measurement. The number of DE counts in the background peak P_{DE} , is used in a relation similar to Eq. (2) to calculate the DE rates [10]. The only difficulty in the analysis is that DE counts and the “trapping” contributions in the MCS are convoluted within one jump. However, one can use the fact that the trapping contribution is time dependent. Initially, at time zero after the cooler jump to the detuning energy at which DE is going to be measured, the number of trapped ions is the same as before the cooler jump. Since the electron energy has been changed, and since the ionization energy changes with electron energy, the number of trapped ions then starts to change. Therefore, the DE contribution is determined by the count rate recorded promptly after the cooler jump.

The variable amount of trapping of ions affects the so-called space charge correction in the electron beam and hence the electron energy on the axis. Because of the absence of phase space cooling, the determination of the “cooling” energy was performed by maximizing the observed DR rate. In principle, the laboratory electron energy is nonlinear [20] due to the space charge of the electron beam as shown in Eq. (3), which gives the energy at the center of the beam:

$$E_e = eU_c - \frac{I_e r_e m_e c^2 (1 - \xi(E_e))}{e v_e} [1 + 2 \ln(b/a)]. \quad (3)$$

The electron current, classical electron radius, electron rest mass, and electron velocity are, respectively, I_e (here 1.45 mA), r_e , $m_e c^2$, and v_e , whereas the diameters of the electron beam and the beam tube are respectively $a=4$ cm and $b=10$ cm. The potential of the cathode U_c is basically the applied voltage V_c minus a contact potential ϕ_c , and $\xi(E_e)$ is a correction to the space charge density due to trapped slow ions originating from ionization of the background gas [11]. For the conditions in CRYRING, $\xi(E_e)$ is of the order of 0.25. Equation (3) is used in an iterative procedure to obtain the correct electron energy. The resulting energy uncertainty is of the order of 0.05 eV at 1.0 eV collision energy.

C. Position- and time-sensitive imaging system

A position- and time-sensitive imaging system records the separation between the fragments, and their arrival-time interval. This detector is positioned 6.3 m behind the electron cooler [12]. DR fragments hit the first of a stack of three

multichannel plates (MCP diameter = 25 mm), the signal from which produces flashes on a phosphor screen. A CCD (charge coupled device) camera is used to image the phosphor and the fragment separation can then be determined. From the distance between the fragments, their kinetic energy is determined which enables [see reactions 1(a)–1(d)] the identification of the dissociation limit. The detailed shape of the distribution of fragment separations over such a detector has been described elsewhere [21]. Timing information is ascertained from gold strips that have been evaporatively coated onto the surface of the last MCP. The strips are translucent to electrons, but the transit of an electron cloud through one of the strips produces enough of a signal so that when amplified, a single channel of a 16-channel constant fraction discriminator (CFD) can be triggered. The timing information is correlated with the correct CCD frame to build the 3D picture. More details can be found in Peterson *et al.* [2]. The method of analysis of the distributions from the imaging detector is the same here as in Ref. [12] on the DR of N_2^+ . A brief resume of that procedure will thus suffice.

The fragments from a DR event that occurs when the molecular axis is aligned with the beam velocity will result in a maximum difference in time and the smallest separation, while those that come from a molecule that is perpendicularly aligned to the beam axis will arrive simultaneously, with the maximum separation. In our spectra the timing measurement is used as a selection criterion, rejecting events that give rise to fragments with an arrival time interval greater than 800 ps. This effectively generates spectra from those events that have their dissociation angle more or less perpendicular to the beam axis, and eliminates the long tails that are a trademark of two-dimensional distance spectrum, in which no timing information is obtained.

We compare observed spectra with model distance distributions in which the finite timing resolution (FWHM \sim 550 ps), and the spatial resolution of the detector (\sim 0.13 mm) are taken into account. Also, the detection efficiency, which is a function of distance due to the ion beam size and the detector size, is taken into account by mapping the effective detector area. For small kinetic energy releases (in this study $<$ 0.6 eV) the rotational temperature gives an observable broadening. We used a 600-K rotational temperature in qualitative accord with the ion source characteristics. A background spectrum (taken with large electron cooler jumps) has been measured separately and is dominated by random coincidences.

III. RESULTS AND DISCUSSION

A. Dissociative recombination

Figure 2 presents the DR rates as a function of the center-of-mass energy. For a given center-of-mass collision energy, one can run the electrons either slower (negative electron energy jumps) or faster (positive electron energy jumps) than the ions. The electron beam at zero collision energy had an energy of only 64.7 eV. Experiments with negative jumps were only possible over a limited range. The center-of-mass collision energies have been corrected for the space charge effect [20] described in Eq. (3). The error bars in the figure are purely statistical at the one σ level and thus represent the *relative* uncertainty, or uncertainty in the *shape* of the curve.

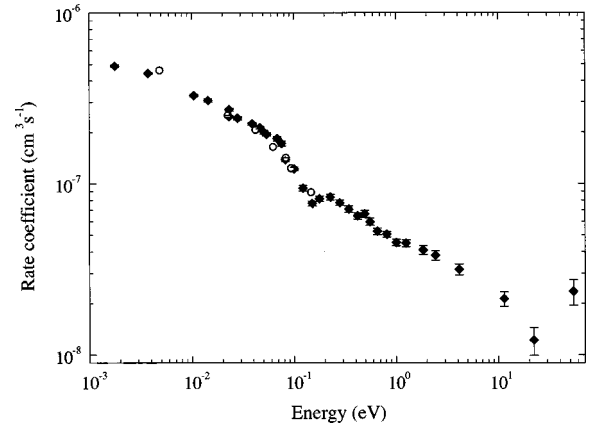


FIG. 2. Absolute dissociative recombination rate coefficient. (\blacklozenge) shows data taken for $v_e > v_{ions}$ and (\circ) shows data taken for $v_e < v_{ions}$. The maximum observed rate defined our zero detuning energy.

In addition to the statistical relative uncertainties, there are also absolute systematic uncertainties which must be considered. The systematic uncertainty in R_B (ion current measurement) is estimated to be about 3% (a new pickup coil [22] has been installed since previous measurements), the circumference is uncertain to less than 1%, the electron current is measured to 2% accuracy, and the current distribution is uncertain [23] to no more than 7%, and the uncertainty in L is estimated to be on the order of 10%. Combining these sources of error yields a total systematic uncertainty of about 13% estimated to be at a level equivalent to one σ . Thus, the whole curve in Fig. 2 could be shifted up or down by 13% within the uncertainty.

The rate coefficient is a convolution of the relative energy distribution with the cross section for DR, $\langle \sigma v \rangle$. Knowing the velocity distribution of the electrons, it is possible to use deconvolution procedures, which have been previously described [10,23] to obtain the DR cross section for CO^+ . Absolute cross-section results are shown in Fig. 3. Figure 3 also contains the single-pass measurements of Mitchell and Hus [14]. This deconvolution procedure sometimes introduces unwanted structures. The magnitudes of the cross sections as well as the power-law energy dependence should be correct, but features in the cross section that do not show up in the rate coefficient should be considered with caution. The structure at 0.15 eV is seen in the rate coefficient data, and is real. The figure also shows the cross section obtained by dividing the rate coefficient with the detuning velocity. The overall energy dependence is found to follow $E_{cm}^{-1.05}$, which is very close to the E_{cm}^{-1} predicted for the “direct” mechanism of DR [24]. The disparity in magnitude between our data and those by Mitchell and Hus [14] is discussed later.

B. Final-state branching ratios

The final state distributions of the fragment from the DR of CO^+ have been measured for four different center-of-mass collision energies. For zero-energy collisions there are four energetically allowed limits, see reactions 1(a)–1(d). For two of the higher collision energies, at 0.4 and 1.0 eV, for which spectra have been measured, there is an additional channel available, leading to the limit $O(^1D) + C(^1D)$ (en-

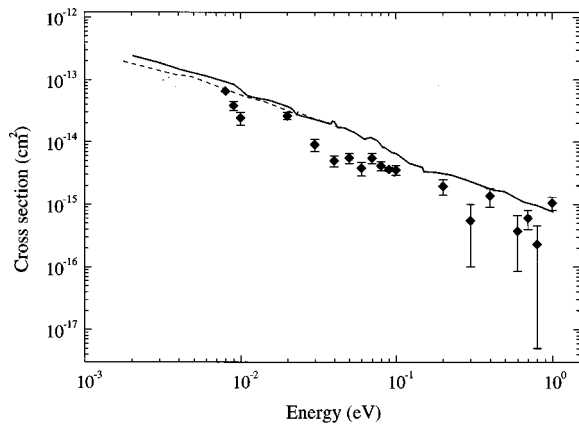


FIG. 3. Absolute dissociative recombination cross section between 1 meV and 1 eV. The full drawn line shows the cross section as derived from the measured rate coefficients, using a deconvolution procedure described in Refs. [10] and [23], with the following electron temperatures: $kT_{\parallel}=0.1$ and $kT_{\perp}=10$ meV. The dashed line shows the cross section derived by dividing the measured rate coefficient by the relative velocity. (\blacklozenge) shows data from Ref. [14].

dothermic at 0 eV collision energy, with an enthalpy change $\Delta H = +0.3$ eV). And for the collision energy of 1.5 eV there is a further limit available resulting in $O(^1S) + C(^3P)$ ($\Delta H = +1.25$ eV).

The distribution of distances measured at 0 eV collisions is shown in Fig. 4. Clearly, it can be seen that at this energy dissociative recombination mostly results in ground-state atomic fragments [$O(^3P) + C(^3P)$]: more than three quarters of all DR events lead to this limit (76%). The least exothermic limit [reaction 1(d)] is not observed. The other two dissociation limits, $O(^3P) + C(^1D)$ and $O(^1D) + C(^3P)$, have yields of 15% and 9%, respectively, see Table I. The error in the fit to the 0-eV spectra is estimated to be $\pm 5\%$ of the branching ratios. It is useful to iterate here that the branching

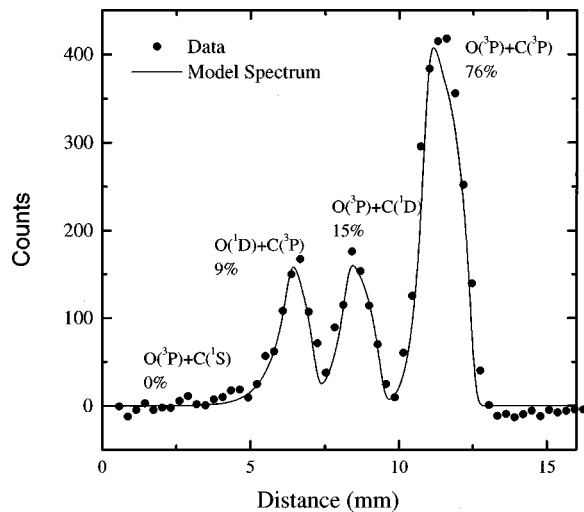


FIG. 4. Distance spectrum for branching fraction determination. (\bullet) shows data taken at 0 eV detuning energy; the full drawn line shows a fit with correction for timing cut off and detector efficiency. Note therefore that the distribution does not directly reflect the branching.

TABLE I. The table shows the final state distribution for four relative collision (detuning) energies. For the 0-eV collision energy the statistical error is about 5%. At the other collision energies, because of less statistics due to lower DR cross sections, the error is 30%.

Limit E_d (eV)	0	0.4	1.0	1.5
$O(^3P) + C(^3P)$	76.1%	53%	39%	38%
$O(^3P) + C(^1D)$	14.5%	34%	35%	35%
$O(^1D) + C(^3P)$	9.4%	8%	15%	11%
$O(^3P) + C(^1S)$	0.0%	0%	5%	5%
$O(^1D) + C(^1D)$		5%	6%	11%
$O(^1S) + C(^3P)$				0%

percentages are the result, for different kinetic energies released, of a modeling procedure that accounts for the beam and detector size, and the different amounts of data rejected, due to the timing selection. Hence, the reported branching ratios do not reflect the intensities in Fig. 4. We note that the distribution spectrum excludes the presence of vibrationally excited CO^+ .

Figure 5 shows the results of the measurements recorded at the collision energies: 0.4, 1.0, and 1.5 eV, respectively. The sharply reduced count rates at elevated electron collision energies is reflected in the reduced quality of the spectra. Independently, a background spectrum has been determined, the shape of which is subtracted. The background intensity was used as a parameter. This has resulted in the negative data points. The data are of reasonable quality and show a clear correlation in the shift and position of the peaks as the collision energy is increased. The trend in branching is thus clear. The extracted branching ratios are also given in Table

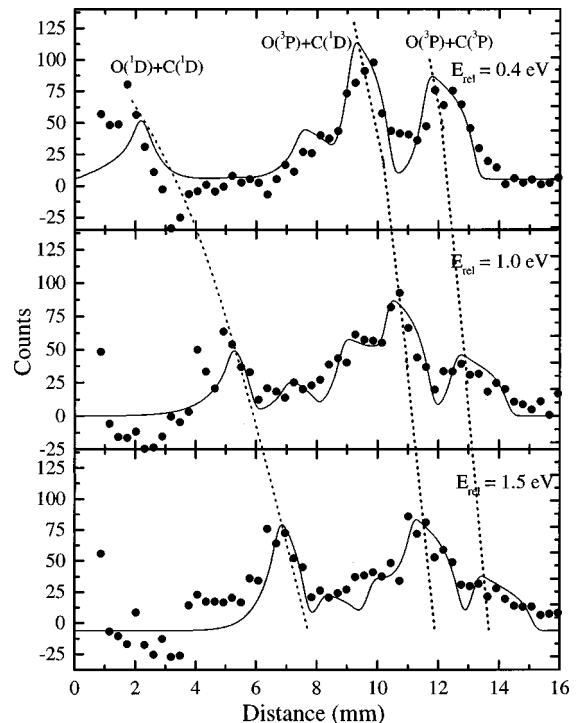


FIG. 5. Distance spectra for various electron collision energies: upper spectrum 0.4 eV; middle spectrum, 1.0 eV; and lower spectrum, 1.5 eV. Note that the best model spectrum in the lower spectrum used an energy of 1.4 eV.

NO^+ , O_2^+ , etc. The reason for this is unclear, however, perhaps part of the reason lies in the difficulty in the measurements using other techniques as is emphasized below. Mentzoni and Donohue [27] apparently made the earliest measurements on what they assumed to be CO^+ using a plasma afterglow method. For electron temperatures of 273 and 800 K, they measured DR rate coefficients of 6.7×10^{-7} and $4 \times 10^{-7} \text{ cm}^3 \text{ s}^{-1}$, respectively. Later, this work was criticized by Whitaker, Biondi, and Johnsen [28] who repeated the experiment, including mass spectrometric identification of ions, and were unable to get a plasma dominated by CO^+ . The main criticism of the work lies in the probable presence of $(\text{CO})_n\text{CO}^+$ clusters, which form readily and are known to recombine rapidly. In general, most of these clusters recombine faster than $1.0 \times 10^{-6} \text{ cm}^3 \text{ s}^{-1}$ at room temperature; for example, one has to consider rate coefficients as large as $1.3 \times 10^{-6} \text{ cm}^3 \text{ s}^{-1}$ for $n=1$ [28] and $1.9 \times 10^{-6} \text{ cm}^3 \text{ s}^{-1}$ for $n=2$ [28]. Thus, it was proposed that such contamination occurred in the experiment by Mentzoni and Donohue and that it could explain their apparent high DR rates.

Mitchell and Hus [14] performed the first merged beams experiment on CO^+ with a single pass setup, and attributed their cross sections to dissociative recombination of electrons with vibrationally excited CO^+ . Later, CO^+ was studied at room temperature by Geoghegan, Adams, and Smith [29] by means of a flowing-afterglow Langmuir-probe apparatus. They reported for CO^+ a rate coefficient of $1.6 \times 10^{-7} \text{ cm}^3 \text{ s}^{-1}$ at room temperature. Although the energy state of the recombining ion is not specified, it is likely to have been the electronic and vibrational ground state, since the pressure was high enough to lead to collisional quenching of excited states.

In order to present a thermal rate coefficient, the DR cross section displayed in Fig. 3 was convoluted with a Maxwellian temperature distribution. The resulting curve is displayed by the solid curve in Fig. 8. This curve can also be represented by the expression

$$\alpha(T_e) = 2.75 \times 10^{-7} \left(\frac{300}{T_e} \right)^{0.55} \text{ cm}^3 \text{ s}^{-1}. \quad (4)$$

Also included are the similarly derived rate coefficients of Mitchell and Hus [14] shown as the dashed curve, and rates discussed above of Mentzoni and Donohue [27] and of Geoghegan, Adams, and Smith [29]. The discrepancy with the data by Geoghegan, Adams, and Smith [29] is not yet explained. These authors used a helium discharge to generate ions and metastable species that consequently ionized Ar, introduced as a test gas downstream. Various possible complications were taken into account, and it is thus difficult to rationalize the factor of 2 difference with the results found in the present work.

B. Mechanisms and interpretations

Our results show that the dissociative recombination of $\text{CO}^+(X^2\Sigma^+)$ is an efficient process, as is the case for all diatomic molecular ions of similar size. For example, at room temperature, thermal rate coefficients for CO^+ , N_2^+ , and O_2^+ are 2.75×10^{-7} , 2×10^{-7} , and $2 \times 10^{-7} \text{ cm}^3 \text{ s}^{-1}$,

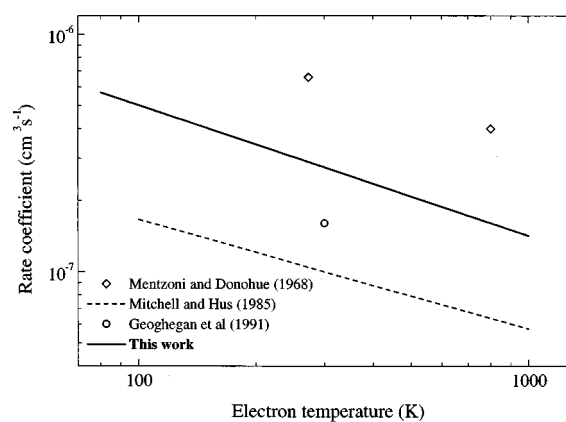


FIG. 8. Thermal rate coefficient. Our work (solid line) and a comparison with literature data from Mentzoni and Donohue [27], Mitchell and Hus [14], and Geoghegan, Adams, and Smith [29].

respectively [12,30,31]. For NO^+ it is even larger [31,32], $3-4 \times 10^{-7} \text{ cm}^3 \text{ s}^{-1}$. The DR process of all these ions are believed to be driven by the so-called “direct” process, which involves curve crossing(s) between the ionic and doubly excited neutral potential curves. The observed rate suggests that this is also the case for CO^+ . The $1/E$ dependence of the cross section (Fig. 3) and the resultant $1/T^{0.5}$ dependence of the thermal rate coefficient [Eq. (4)] is not in contradiction [24] with a direct mechanism with a favorable Franck-Condon overlap. In the discussion below we will attempt to mention some possible neutral states.

Before proceeding with that discussion, however, it is important to recognize that there is evidence for some contributions to the observed rates from the so-called “indirect process.” The “indirect” process is known to induce dips in the cross section due to destructive interference with DR through the “direct” process. The feature at 0.15 eV in Fig. 2 may be an example. As already noted, N_2^+ is isoelectronic with CO^+ . Guberman [33] included both “direct” and “indirect” processes to calculate the cross sections for the dissociative recombination of $\text{N}_2^+(X^2\Sigma_g^+)$ up to 1 eV wherein he predicted some dips that were not observed in our study [12] of that ion. From all possible explanations, we believe that such features may have been smeared out, because of the large number of target ion states with vibrational states up to $v=3$. Nitrogen ions are infrared inactive, and do not cool radiatively in contrast to CO^+ .

Turning our attention again to the direct mechanism, we note that no calculations immediately relevant to the DR mechanism have so far been carried out to our knowledge. Some work on photodissociation of CO above the ionization energy may be the same channels used in the DR of CO^+ . For the discussion, we refer to Fig. 9 where some of the curves discussed are displayed. It was found [34,35] that photodissociation of CO does not proceed through direct excitation to repulsive states, but rather by dissociation of bound Rydberg states. For example, the $n s \sigma$ and the $n p \sigma$ series converging to the $\text{CO}^+(X^2\Sigma^+)$ state were investigated [36] (up to $n=6$). The first member of the $n s \sigma$ series, the $B^1\Sigma^+$ states, is predissociated by the $D'^1\Sigma^+$ valence state [37–39]. Adiabatically, the B and D' states form a

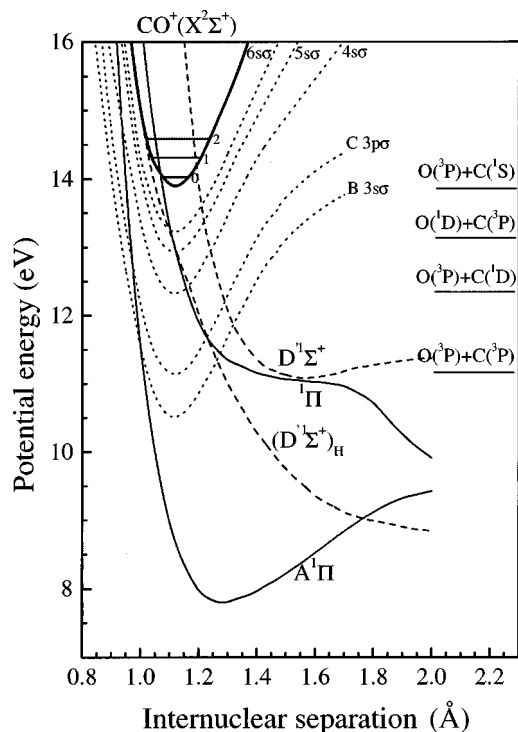


FIG. 9. Potential energy curves, which may be relevant for dissociative recombination, taken from Refs. [40] ($D' \ ^1\Sigma^+$) and [42] ($D' \ ^1\Sigma^+_{\text{H}}$ and $^1\Pi$).

double minimum potential curve. The D' state correlates asymptotically with the $O(^3P) + C(^3P)$ ground-state limit. The (diabatic) $D' \ ^1\Sigma^+$ state is considered to be responsible for the predissociation of the $(3s\sigma) B \ ^1\Sigma^+(v=2)$ [40], the $(3p\sigma) C \ ^1\Sigma^+(v=3,4)$ [40], and the $(4p\sigma) K \ ^1\Sigma^+(v=0)$ [41] states. In a similar manner, the $E \ ^1\Pi(v=0)$ [first member of the $np\pi$ series (not shown)], the $(4p\pi) L \ ^1\Pi(v=0)$ and the $(3d\pi) L' \ ^1\Pi(v=1)$ Rydberg states are predissociated by interaction with a dissociative state of the $^1\Pi$ symmetry [42] shown simply by this notation in Fig. 9. The $^1\Pi$ and $D' \ ^1\Sigma^+$ states are invoked by Hiyama and Nakamura [42] to be involved in the “direct” dissociative recombination mechanism. It is of interest to note that a strong coupling between Rydberg states and a repulsive doubly excited valence state directly implies a large electron capture width of the repulsive state in the ionization continuum and hence a possible important role in the DR process.

It is conventional wisdom that for the direct DR process to be efficient at low energies, there must be a crossing of a repulsive neutral curve through the lower part of the ionic curve. The internuclear separation at the crossing is also generally regarded as important. Figure 9 shows a large discrepancy between the position of the $(D' \ ^1\Sigma^+)_{\text{H}}$ state of Hiyama and Nakamura [42] and the same state reported by Tchang-Brillet *et al.* [40], labeled $D' \ ^1\Sigma^+$. According to Hiyama and Nakamura, the position of their calculated D' state should be accurate to within 0.027 eV, whereas the $^1\Pi$ state is supposed to be accurate within 0.14 eV. The location of both of these calculated curves is toward the inner wall of the ionic curve. The D' state of Tchang-Brillet *et al.* [40], which was deduced from spectroscopic data, crosses the ionic curve toward the outer wall. In considering “direct” dissociative recombination to such states, the efficiency of

the process is favored if the crossing is toward the outer wall of the ionic potential curve over the case where it is toward the inner wall. In view of the absence of sufficiently accurate curves and a complete absence of information on the triplet states, we cannot make any detailed comparison between our findings and the quality of the mentioned neutral states. Moreover, all of the above only takes into consideration ground-state fragments, whereas we observe other dissociation limits. Ebata, Sutani, and Mikami [43] pointed out that the $O(^1D) + C(^3P)$ and $O(^3P) + C(^1D)$ dissociations should proceed through a spin-orbit coupling if the capture state is a singlet state. According to O’Neil and Schaefer [44], the $(2,3,4,5)^3\Sigma^+$ states are all repulsive and go respectively to $O(^3P) + C(^3P)$, $O(^3P) + C(^1D)$, $O(^1D) + C(^3P)$, and $O(^3P) + C(^5S)$. Clearly the theory is in its infancy, and much work is required.

In examining Fig. 2, one sees that a high energy resonance is not observed as is found in some light species such as the H_3^+ isotopomers [45,46] and HeH^+ [10]. However, such features have not been seen before for “heavier” ions such as C_2^+ and C_3^+ [47] or for N_2^+ [12], but are present in NO^+ , and O_2^+ . We note that the single point at 54 eV lies a factor of 2 higher than that at 22.3 eV. It is unlikely that this is the start of a high energy “bump,” as the 54-eV point lies well into the multiple ionization continuum for the species. At this energy one can imagine strong autoionization processes to be present.

Using the $^1\Pi$ state of Hiyama and Nakamura [42] and the $D' \ ^1\Sigma^+$ state of Tchang-Brillet *et al.* [40] we have performed overlap integrals between CO^+ in its ground vibrational state. The different electron collision energies were accounted for by evaluating the overlap integral with the continuum state at the total energy of $CO^+(v=0) + e^-$. This calculation provides a rough qualitative idea of the behavior of the capture probability of these states with increasing electron energy. It is found that with increasing energy, the overlap integral to the $D' \ ^1\Sigma^+$ state increases, while that to the $^1\Pi$ state decreases. In going from zero energy to 0.8 eV the Franck-Condon factor reduces by more than one half. These findings are very qualitative but may indicate that at zero energy it is the $^1\Pi$ state that is the predominant repulsive state involved in the DR, while at higher energy it is the $D' \ ^1\Sigma^+$ state that becomes more important.

V. SUMMARY AND CONCLUSIONS

The ion storage ring measurement of dissociative recombination of CO^+ shows that DR is a very efficient process. Cross sections of about $4 \times 10^{-12} \text{ cm}^2$ at 1 meV and 10^{-15} cm^2 at 1 eV are found, with an essentially $1/E$ dependence. Thermal rate coefficients previously appearing in the literature differ from one another by up to a factor of 6. Our deduced value of $2.75 \times 10^{-7} (300/T_e)^{0.55} \text{ cm}^3 \text{ s}^{-1}$ lies in between previous measurements. The disparity with some of the other measurements can be rationalized. The rate coefficient is about 1.7 times larger than the value for the isoelectronic ion. The experimental results from the imaging detector indicate that at zero collision energy the DR mechanism is dominated by a direct dissociation process to the ground-state [76% branching to $O(^3P) + C(^3P)$]. As the collision energy is increased the branching fraction to the ground-state

limit is found to decrease rapidly. Between 0 and 0.4 eV, DR of CO⁺ yields 15–30 % of C(¹D) atoms, in contrast to the 100% at 300 K assumed by Feldman [4,5] to explain UV lines in comets Kahoutek and West.

The cross section for dissociative excitation of CO⁺ was also measured. The magnitude of the cross section after rising from threshold somewhere around 12.5 eV, is very typical of dissociative excitation cross sections $\approx 2 \times 10^{-16}$ cm². In the present work the quality of the SBD prevented determining the branching between the two dissociative excitation channels, C⁺+O and C+O⁺.

There is a large disparity in the literature concerning the position of the dissociative states that would be involved in DR for this ion. It is clear that a great deal more remains to be done on the theoretical side. The present information prevents even a qualitative interpretation of the observation in terms of potential energy curves. These results provide an opportunity for theorists to address the dissociative recombination process of a moderate sized ion that is fully relaxed to the ground electronic and vibrational states. It should be all

the more attractive since it is isoelectronic with N₂⁺, which has been widely studied theoretically, but has not yielded to experimental high resolution studies of fully ground-state ions.

ACKNOWLEDGMENTS

The authors are grateful to Brian Mitchell for discussions on this work, especially as it relates to his earlier work. The staff members of the Manne Siegbahn Laboratory are gratefully acknowledged for valuable help with the experiments. The work was supported in part by the Göran Gustafsson Foundation and the Swedish Natural Science Research Council. One of us (G.H.D.) was supported in part by the Swedish Royal Academy of Sciences and by the U.S. Department of Energy. Two of us (W.J.v.d.Z. and R.P.) acknowledge financial support from the Netherlands Organization of Scientific Research (NWO). This work is part of the scientific program of the Netherlands Foundation for Fundamental Research (FOM).

-
- [1] N. R. Erickson, R. L. Snell, R. B. Loren, L. Mundy, and R. L. Plambeck, *Astrophys. J. Lett. Ed.* **245**, L83 (1981).
- [2] H. Störzer, J. Stutzki, and A. Sternberg, *Astron. Astrophys.* **296**, L9 (1995).
- [3] A. Fuente and J. Martin-Pintado, *Astrophys. J. Lett.* **477**, L107 (1997).
- [4] P. D. Feldman, *Astron. Astrophys.* **70**, 547 (1978).
- [5] P. D. Feldman and W. H. Brune, *Astrophys. J. Lett.* **209**, L145 (1976).
- [6] H. Balsiger, K. Altwegg, F. Bühler, J. Geiss, A. G. Ghielmetti, B. E. Goldstein, R. Goldstein, W. T. Huntress, W. H. Ip, A. J. Lazarus, A. Meier, M. Neugebauer, U. Rettenmund, H. Rosenbauer, R. Schwenn, R. D. Sharp, E. G. Shelley, E. Ungstrup, and D. T. Young, *Nature (London)* **321**, 330 (1986).
- [7] M. B. McElroy, T. Y. Kong, and Y. L. Yung, *J. Geophys. Res.* **82**, 4379 (1977).
- [8] M. K. Wallis, *Planet. Space Sci.* **26**, 949 (1978).
- [9] A. O. Nier and M. B. McElroy, *Science* **194**, 1298 (1976).
- [10] C. Strömholm, J. Semaniak, S. Rosén, H. Danared, S. Datz, W. J. van der Zande, and M. Larsson, *Phys. Rev. A* **54**, 3086 (1996).
- [11] C. Strömholm, H. Danared, Å. Larson, M. Larsson, C. Marian, S. Rosén, B. Schimmelpfennig, I. F. Schneider, J. Semaniak, A. Suzor-Weiner, U. Wahlgren, and W. J. van der Zande, *J. Phys. B* **30**, 4919 (1997).
- [12] J. R. Peterson, H. Danared, G. H. Dunn, M. Larsson, A. Le Padellec, Å. Larson, R. Peverall, C. Strömholm, S. Rosén, M. af Ugglas, and W. J. van der Zande, *J. Chem. Phys.* **108**, 1978 (1998).
- [13] H. Danared, *Nucl. Instrum. Methods Phys. Res. A* **335**, 397 (1993).
- [14] J. B. A. Mitchell and H. Hus, *J. Phys. B* **18**, 547 (1985).
- [15] J. Desquelles, M. Dufay and D. C. Poulizac, *Phys. Lett.* **27A**, 96 (1968).
- [16] R. G. Bennett and F. W. Dalby, *J. Chem. Phys.* **31**, 434 (1959).
- [17] G. R. Möhlmann and F. J. De Heer, *Chem. Phys. Lett.* **43**, 170 (1976).
- [18] R. F. Holland and W. B. Maier, *J. Chem. Phys.* **56**, 5229 (1972).
- [19] C. M. Marian, M. Larsson, B. J. Olsson, and P. Sigraý, *Chem. Phys.* **130**, 361 (1989).
- [20] Kilgus, D. Habs, D. Schwalm, and A. Wolf, *Phys. Rev. A* **46**, 5730 (1992).
- [21] D. Zajfman, Z. Amitay, C. Broude, P. Forck, B. Seidel, M. Grieser, D. Habs, D. Schwalm, and A. Wolf, *Phys. Rev. Lett.* **75**, 814 (1995).
- [22] BERGOZ Beam Charge Monitor, 01170 Crozet, France. Model BCM-CA #041. This device was custom made for MSL. It is about 10 times more sensitive than the previous MSL device. It was calibrated against the old monitor which, in turn, was calibrated with a current in a loop to an accuracy of about 2%.
- [23] L. H. Andersen, J. Bolko, and P. Kvistgaard, *Phys. Rev. A* **41**, 1293 (1990). Also, A. Wolf (private communication).
- [24] D. R. Bates, *Phys. Rev.* **78**, 492 (1950).
- [25] W. J. van der Zande, J. Semaniak, V. Zengin, G. Sundström, S. Rosén, C. Strömholm, S. Datz, H. Danared, and M. Larsson, *Phys. Rev. A* **54**, 5010 (1996).
- [26] N. Honjou and F. Sasaki, *Mol. Phys.* **37**, 1593 (1979).
- [27] M. H. Mentzoni and J. Donohoe, *Phys. Lett.* **26A**, 330 (1968).
- [28] M. Whitaker, M. A. Biondi, and R. Johnsen, *Phys. Rev. A* **23**, 1481 (1981).
- [29] M. Geoghegan, N. G. Adams, and D. Smith, *J. Phys. B* **24**, 2589 (1991).
- [30] F. J. Mehr and M. A. Biondi, *Phys. Rev. A* **181**, 264 (1969).
- [31] P. Spanel, L. Dittrichova, and D. Smith, *Int. J. Mass Spectrom. Ion Processes* **129**, 183 (1993).
- [32] P. M. Mul and J. Wm. McGowan, *J. Phys. B* **12**, 1591 (1979).
- [33] S. L. Gubermann, in *Dissociative Recombination: Theory, Experiment, and Applications*, edited by B. R. Rowe, J. B. A. Mitchell, and A. Canosa, Vol. 313 of *NATO Advanced Study Institute Series B: Physics* (Plenum, New York, 1993), p. 47.
- [34] C. Letzelter, M. Eidelsberg, F. Rostas, J. Breton, and B.

- Thiebelmont, *Chem. Phys.* **114**, 273 (1987).
- [35] Y. P. Viala, C. Letzelter, M. Eidelsberg and F. Rostas, *Astron. Astrophys.* **193**, 265 (1988).
- [36] M. Eidelsberg and F. Rostas, *Astron. Astrophys.* **235**, 472 (1990).
- [37] M. Eidelsberg, J. Y. Roncin, A. Le Floch, F. Launay, C. Letzelter, and J. Rostas, *J. Mol. Spectrosc.* **121**, 309 (1987).
- [38] D. M. Cooper and S. R. Langhoff, *J. Chem. Phys.* **74**, 1200 (1981).
- [39] G. L. Wolk and J. W. Rich, *J. Chem. Phys.* **79**, 12 (1983).
- [40] W.-Ü. L. Tchang-Brillet, P. S. Julienne, J. M. Robbe, C. Letzelter, and F. Rostas, *J. Chem. Phys.* **96**, 6735 (1992).
- [41] M. Drabbels, J. Heinze, J. J. Ter Meulen, and W. L. Meerts, *J. Chem. Phys.* **99**, 5701 (1993).
- [42] M. Hiyama and H. Nakamura, *Chem. Phys. Lett.* **248**, 316 (1996).
- [43] T. Ebata, T. Sutani, and N. Mikami, *Chem. Phys. Lett.* **240**, 357 (1995).
- [44] S. V. O'Neil and H. F. Schaefer, *J. Chem. Phys.* **53**, 3994 (1970).
- [45] G. Sundström, J. R. Mowat, H. Danared, S. Datz, L. Broström, A. Filevich, A. Källberg, S. Mannervik, K. G. Rensfelt, P. Sigra, M. af Ugglas, and M. Larsson, *Science* **263**, 785 (1994).
- [46] S. Datz, M. Larsson, C. Strömholm, G. Sundström, V. Zengin, H. Danared, A. Källberg, and M. af Ugglas, *Phys. Rev. A* **52**, 2901 (1995).
- [47] P. Forck, Ph.D. thesis, University of Heidelberg, 1994.